Journal of Solid State Chemistry 181 (2008) 1824–1832

Contents lists available at ScienceDirect

Journal of Solid State Chemistry

journal homepage: www.elsevier.com/locate/jssc

Effect of oxygen non-stoichiometry on the structural and magnetotransport properties of $LaMn_{0.85}Cr_{0.15}O_{3+\delta}$

Liliana B. Morales [a], Roberto Zysler [a], Alberto Caneiro [a,b,*]

[a] CONICET, Argentina
[b] Centro Atómico Bariloche, Instituto Balseiro, 8400 S. C. de Bariloche, Río Negro, Argentina

ARTICLE INFO

Article history:
Received 24 December 2007
Received in revised form
14 March 2008
Accepted 13 April 2008
Available online 20 April 2008

Keywords:
Oxygen non-stoichiometry
Cr-doped manganite
Perovskite structure
Magnetoresistance

ABSTRACT

Thermogravimetry, X-ray diffraction (XRD), d.c. magnetization, high-temperature susceptibility and electrical resistivity measurements were performed for $LaMn_{0.85}Cr_{0.15}O_{3+\delta}$ perovskites with accurate control of the oxygen content ($0 \leqslant \delta \leqslant 0.11$). For $0 \leqslant \delta < 0.09$, three orthorhombic structures (*Pnma*) are found: for $0 \leqslant \delta < 0.045$, the O′ phase ($b/\sqrt{2} < c < a$), for $0.045 \leqslant \delta < 0.06$, the O″ ($b/\sqrt{2} < a < c$) and for $0.06 \leqslant \delta < 0.09$, the O‴ ($a < b/\sqrt{2} < c$). For $0.09 \leqslant \delta \leqslant 0.11$, a rhombohedral symmetry ($R\bar{3}c$) coexists with O‴ in a biphasic field. Magnetic measurements revealed the ferromagnetic interactions (FM) character of the Mn^{3+}–O–Cr^{3+} interaction, but also the intricate magnetic phase diagram due to the presence of multiple interactions ($Mn^{3+,4+}$–O–$Mn^{3+,4+}$, Cr^{3+}–O–Mn^{3+}, etc.). The comparison of the results for $LaMn_{0.85}Cr_{0.15}O_{3+\delta}$ with those of $LaMn_{0.9}Cr_{0.1}O_{3+\delta}$ allows discuss the role of Cr^{3+} on the structural, magnetic and magnetotransport properties of the $LaMn_{1-x}Cr_xO_{3+\delta}$ perovskites.

1. Introduction

Compounds with perovskite structure are extensively studied due to their wide range of interesting properties. The ideal cubic perovskite structure, ABX_3, (S.G.$Pm\bar{3}m$) consists essentially of a framework of BX_6 octahedra linked by their corners, with a large 12 coordinated *A* cation. If the *A*, *B*, and *X* ions are not of ideal relative size, structural distortions occur and depend on the sizes and bonding character of the cations. In these compounds, the magnetic cation–anion–cation exchange interaction depends on the electron configuration of the *B* cations and on both, the *B*–O distances and the *B*–O–*B* bond angles. The strength of the magnetic exchange interaction is strongly dependent on the magnitude of the bond angle [1].

There has been substantial interest in the $LaMnO_{3+\delta}$ perovskite due to the rich magnetic phase diagram and the relationship with structural distortions induced by variation of oxygen content [2,3]. The stoichiometric compound has O′ orthorhombic symmetry ($b/\sqrt{2} < c < a$) with *A*-type antiferromagnetic order. This order consists of ferromagnetic (FM) interactions in the (001) plane and AFM interactions between them. This magnetic configuration is related to orbital ordering between empty and occupied e_g states in the a–b plane and AFM superexchange (SE) interactions between two manganese with three half-filled t_{2g} orbitals. $LaMnO_{3.00}$ contains trivalent manganese and due to the strong Hund's coupling, these ions adopt a high spin configuration $t_{2g}^3\, e_g^1$. According to the Jahn–Teller theorem, a distortion of the local octahedral environment is energetically favorable. This distortion is accomplished by lengthening two of the Mn–O bonds, which lowers the energy of the occupied $3d_z^2$ orbital, relative to the empty $3d_{x^2-y^2}$ [1]. A small FM component is always present due to the antisymmetric Dzialoshinski exchange coupling ($\mathbf{D}_{ij} \cdot \mathbf{S}_i \times \mathbf{S}_j$) introduced by the tilt of the MnO_6 octahedra leading to a weak-ferromagnetic phase.

The cooperative Jahn–Teller distortion (JTD) can be suppressed increasing either the temperature or the oxygen content. The latter changes the average Mn valence (Mn^{3+}–Mn^{4+}) raising the hole concentration, i.e. the empty e_g levels. Thus, increasing Mn^{4+} concentration favors FM order due to the Mn^{3+}–O–Mn^{4+} double exchange (DE) interaction and the progressive remove of JTD. The CMR process in manganites is associated with the DE mechanism as a result of the motion of the e_g electron [4,5]. This concept is usually applied when a mixed valence ion is present. The substitution of Mn ions (by Cr, Sn, Co, Ni, Fe, etc.) alters the magnetic interactions in the Mn–O network and therefore the magnetic phase diagram. For this reason, these substitutions have been extensively studied [6–9]. This is also another way to fully understand the origin of the magnetoresistance effect.

In Cr-doped manganites, chromium is incorporated as Cr^{3+} in the *B* site of the perovskite structure. Since Cr^{3+} is isoelectronic with Mn^{4+} ($3d^3$–$t_{2g}^3 e_g^0$) it could play a similar role in the DE

* Corresponding author at: Centro Atómico Bariloche, Instituto Balseiro, 8400 S. C. de Bariloche, Río Negro, Argentina. Fax: +54 2944445274.
E-mail address: caneiro@cab.cnea.gov.ar (A. Caneiro).

0022-4596/$ - see front matter © 2008 Elsevier Inc. All rights reserved.
doi:10.1016/j.jssc.2008.04.008

mechanism as Mn^{4+}. The role of Cr^{3+} in the magnetism of $LaMn_{1-x}Cr_xO_3$ has been discussed in the literature in recent years. An early neutron diffraction study of the $LaMn_{1-x}Cr_xO_3$ solid solution indicates that the *A*-type AFM structure of $LaMnO_3$ persists only for very small concentrations of Cr^{3+}, while the *G*-type AFM of $LaCrO_3$ is found over a wide compositional range. The introduction of Cr^{3+} into the *A*-type AFM structure leads to a spin reversal of some of the Mn^{3+} nearest neighbors increasing the ferromagnetic moment [10]. Later some authors suggested a ferromagnetic Cr^{3+}–O–Mn^{3+} exchange interaction (SE or DE) since Cr^{3+} is isoelectronic with Mn^{4+} [11–15]. However, it has been claimed that the effective DE interaction cannot be established between Cr^{3+} and Mn^{3+} ions and only the SE takes place [16,17]. A recent publication suggests the presence of two different DE processes in this system: a strong Mn^{3+}–O–Mn^{4+} DE interaction and a weak Mn^{3+}–O–Cr^{3+} one [18,19]. The AFM character of this interaction has been also suggested by others authors [20]. More recently, the effect of Cr substitution on samples free of Mn^{4+} was reported by Morales et al. [21]. With the help of a simple model, it was possible to explain the presence of magnetoresistance by the appearance of a gap between Mn^{3+} and Cr^{3+} electronic bands that becomes smaller by increasing Cr content and applying an external magnetic field. This model proposes the necessity of DE mechanism between Mn^{3+} and Cr^{3+} to explain the high values of the observed magnetoresistance.

It is worth mentioning that in most of the studies carried out on $LaMn_{1-x}Cr_xO_3$ ($0<x<1$) samples, the effect of oxygen content on the crystal structure and magnetic behavior has not been analyzed in detail.

The paper is aimed at reporting a systematic study of the magnetic and transport properties and its interplay with the structural features of the $LaMn_{1-x}Cr_xO_{3+\delta}$ system as a function of chromium, x, and oxygen content, $3+\delta$. For this purpose, the δ values were varied over a wide range ($0\leqslant\delta\leqslant0.11$) for $x=0.15$ and both, the evolution of the crystal structure and the magnetic response were followed. The results presented here are discussed in comparison with previous ones obtained for $LaMn_{0.90}Cr_{0.10}O_{3+\delta}$ ($0\leqslant\delta\leqslant0.12$) compositions [22]. This comparison allows to clarify the role of Cr^{3+} on the structural, magnetic and magnetotransport properties of the $LaMn_{1-x}Cr_xO_{3+\delta}$ perovskites.

2. Experimental

Samples of nominal composition $LaMn_{0.85}Cr_{0.15}O_3$ were synthesized following the liquid-mix method [23] using La_2O_3, CrO_3, and metallic Mn (all reactants with purity higher than 99.9%) as reagents. The phase was prepared in the same way as reported elsewhere [22] and synthesized at 1000 °C for 12 h in air. By in-situ high-temperature X-ray diffraction (XRD), it was found that, for $T>1050$ °C in air, a secondary phase $(Cr, Mn)_3O_4$ is precipitated. Prior to use, La_2O_3 and CrO_3 were thermally treated in order to remove absorbed or chemically bonded products such as CO_2 and H_2O.

XRD patterns were collected on a Philips PW-1700 diffractometer using Cu$K\alpha$ radiation and a graphite monochromator. The structural refinements were carried out using the Rietveld method (Fullprof) [24]. For this purpose, the diffractograms were collected in the $20^\circ\leqslant2\theta\leqslant120^\circ$ range, with steps of 0.02° and counting time of 15 s per step.

Equilibrium $p(O_2)$ measurements as a function of $3+\delta$ and temperature, T, were performed using thermogravimetric (TG) equipment consisting of a symmetrical thermobalance based on a Cahn 1000 electrobalance coupled to an electrochemical system [25]. Samples with controlled oxygen content ($3.00\leqslant3+\delta\leqslant3.11$) were prepared by annealing at different temperatures and $p(O_2)$ values for 24 h and then quenching in liquid nitrogen. We handle a highly accurate method to control the oxygen content of non-stoichiometric oxides. This method was used previously to study several complex oxide systems [3,22,26,27]. Although oxygen excess in the perovskite structure is not possible due to its compact character, in the present work the oxygen content is expressed as $3+\delta$ just for clarity instead of the chemical formula $La_{3/3+\delta}(Mn_{0.85}Cr_{0.15})_{3/3+\delta}O_3$.

Magnetization (M) data were measured between 5 and 300 K under an applied magnetic field (H) of 0.01 T and at 5 K with $-5\,T\leqslant H\leqslant5\,T$. Both kinds of measurement were made in a SQUID magnetometer (quantum design). The electrical resistance (R) vs. T was obtained by the four-probe method with both $H=0$ and 7 T.

3. Results and discussion

3.1. Oxygen non-stoichiometry

The TG curve for the $LaMn_{0.85}Cr_{0.15}O_{3+\delta}$ compound was measured in order to determine the range of oxygen non-stoichiometry. The $\log\{p(O_2)/atm\}$ dependence as a function of $3+\delta$ for the 1000 °C isotherm is plotted in Fig. 1. The curve corresponding to $LaMnO_{3+\delta}$ is also included for comparison. The rapid variation of $p(O_2)$ for $\log\{p(O_2)/atm\}<-5$ indicates the existence of the stoichiometric $LaMn_{0.85}Cr_{0.15}O_{3.00}$ compound. Considering that the oxygen stoichiometric phase is formed at 1000 °C within the range $-7<\log\{p(O_2)/atm\}<-5$ it is possible to accurately determine the absolute oxygen concentration of samples as a function of $p(O_2)$. Extra data points (900, 800, and 700 °C) taken under pure oxygen were added in Fig. 1 to show the increase in oxygen content as the temperature decreases.

Oxygen non-stoichiometry of this compound is clearly revealed through the shape of the obtained curve. This fact obviously shows the importance of the synthesis procedure and the correct characterization of the samples. The oxygen non-stoichiometry for $LaMn_{0.85}Cr_{0.15}O_{3+\delta}$ is smaller than that of the $LaMnO_{3+\delta}$ compound but it is still very significant. By comparison with the curve presented by Morales and Caneiro [22] for $LaMn_{0.9}Cr_{0.1}O_{3+\delta}$ the oxygen non-stoichiometry decreases as the Cr content increases, which is in agreement with the fact that the pure $LaCrO_3$ phase is stoichiometric in oxygen.

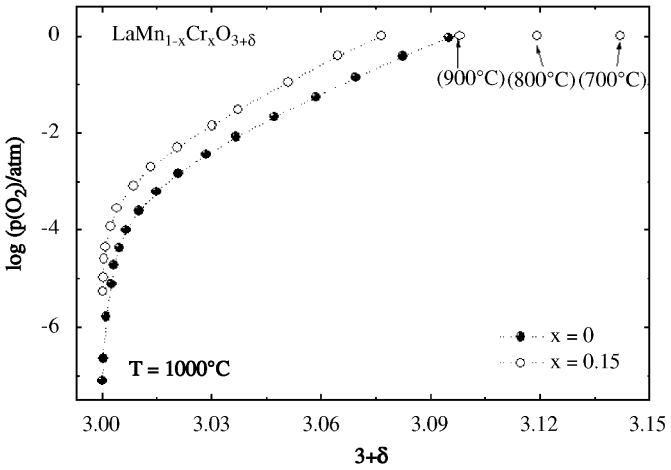

Fig. 1. Comparison between isotherms of $\log\{p(O_2)/atm\}$ vs. oxygen content ($3+\delta$) of $LaMnO_{3+\delta}$ and $LaMn_{0.85}Cr_{0.15}O_{3+\delta}$ at $T=1000$ °C. Extra points under pure oxygen at lower temperatures are included and marked in this plot.

3.2. Structural characterization

The XRD profiles at room temperature indicated that all samples ($0 \leqslant \delta \leqslant 0.11$) were single phase in the sense that impurity phases were not detected (Fig. 2). This was confirmed by microanalysis techniques (SEM–EDS) where agreement with the cation stoichiometry was established. For $0 \leqslant \delta < 0.09$, the studied samples displayed orthorhombic symmetry. Those with $0.09 \leqslant \delta < 0.11$ revealed the existence of a biphasic field where orthorhombic and rhombohedral symmetries coexist.

Henceforth, the ions at the *B*-site of the perovskite structure ($Mn^{3+,4+}$ and Cr^{3+}) will be referred as *B* (both cations occupy the same crystallographic site).

The results of structural refinements are presented in Tables 1 and 2. The structure of samples with orthorhombic symmetry was refined using space group *Pnma* with La^{3+} in position $4(c) = (x, 1/4, y)$, *B* cations in $4(b) = (0,0,1/2)$, O in $4(c)$ and $8(d) = (x, y, z)$. This symmetry is characterized by the cooperative buckling of corner-shared octahedra decreasing the cation–anion–cation angle: in plane this rotation is given by the rotation angle $\omega = (180\text{-}B\text{–}O_2\text{–}B)/2$, O_2 being the in-plane oxygen (see Fig. 3). Between planes the rotation is described by the tilt angle $\varphi = (180\text{-}B\text{–}O_1\text{–}B)/2$, with O_1 being the apical oxygen. In addition, the cooperative Jahn–Teller effect causes the deformation of the octahedra and for this reason, there exists three different distances: in-plane, the long distance $d^l = d(B\text{–}O_2)^l$ and the short $d^s = d(B\text{–}O_2)^s$, and between planes the medium distance $d^m = d(B\text{–}O_1)^m$ (see Fig. 3). As the distortion decreases, the transition to the rhombohedral symmetry occurs where the rotation and tilt angles are equal and the octahedra are regular. In this case the space group used was $R\bar{3}c$ (in hexagonal axes) with La^{3+} in position $6(a) = (0, 0, 1/4)$, *B* cations in $6(b) = (0,0,0)$, and O in $18(e) = (x, 0,1/4)$.

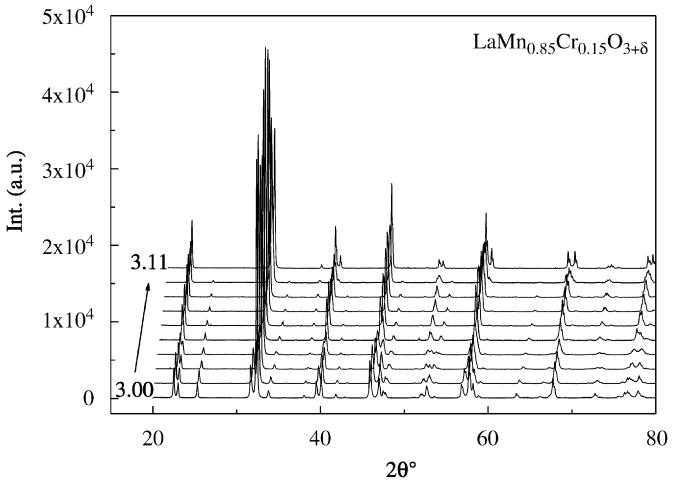

Fig. 2. X-ray powder diffraction data of the studied samples ($3+\delta = 3.00$, 3.01, 3.02, 3.03, 3.04, 3.05, 3.06, 3.07, 3.09, and 3.11). No impurity phases were detected in all of them.

Table 1
Variation of cell parameters, volume, and symmetry as a function of oxygen content

$3+\delta$	Symmetry	a (Å)	b^* (Å)	c (Å)	Vol. (Å^3)
3.00	O′ ($b^*<c<a$)	5.6509(1)	5.4742(1)	5.5369(1)	242.351(4)
3.01	O′ ($b^*<c<a$)	5.6287(2)	5.4801(2)	5.5361(2)	241.502(4)
3.02	O′ ($b^*<c<a$)	5.5996(1)	5.4950(1)	5.5393(2)	241.043(4)
3.03	O′ ($b^*<c<a$)	5.5914(1)	5.4965(3)	5.5382(2)	240.709(4)
3.04	O′ ($b^*<c<a$)	5.5488(1)	5.5091(1)	5.5346(1)	239.263(4)
3.05	O″ ($b^*<a<c$)	5.5265(1)	5.5156(1)	5.5364(1)	238.661(4)
3.06	O‴ ($a<b^*<c$)	5.5145(1)	5.5173(1)	5.5393(1)	238.345(4)
3.07	O‴ ($a<b^*<c$)	5.5056(1)	5.5124(1)	5.5375(1)	237.669(4)
3.09	O‴ ($a<b^*<c$)	5.5036(1)	5.5096(1)	5.544 (1)	237.742(4)
	R	5.5401(1)		5.4615(1)†	355.742(4)
3.11	O‴ ($a<b^*<c$)	5.4853(1)	5.4968(1)	5.5283(1)	235.735(4)
	R	5.5305(1)		5.4446(1)†	353.267(4)

$b^* = b/\sqrt{2}$ for the orthorhombic symmetry (S.G. *Pnma*) and $c\dagger = c/\sqrt{6}$ for the rhombohedral (S.G. $R\bar{3}c$).

Table 2
Evolution as a function of oxygen content of the structural distortion

$3+\delta$	d^m (Å)	d^l (Å)	d^s (Å)	s	φ (deg.)	ω (deg.)
3.00	1.979(6)	2.115(8)	1.922(3)	0.911	12.0(1)	11.5(1)
3.01	1.980(3)	2.103(7)	1.923(6)	0.914	11.8(1)	11.4(1)
3.02	1.984(2)	2.085(6)	1.924(6)	0.919	11.7(1)	10.8(1)
3.03	1.983(2)	2.084(4)	1.922(5)	0.920	11.4(1)	10.8(1)
3.04	1.985(2)	2.043(7)	1.939(7)	0.926	11.1(1)	10.3(1)
3.05	1.985(1)	1.991(8)	1.981(8)	0.943	10.8(1)	10.1(1)
3.06	1.984(1)	1.999(7)	1.986(8)	0.945	10.6(1)	9.9(1)
3.07	1.980(1)	1.982(7)	1.978(7)	0.947	10.2(1)	9.6(1)

Distances between *B*-site cation and oxygen, ($d^m = d(B\text{–}O_1)^m$, $d^l = d(B\text{–}O_2)^l$, and $d^s = d(B\text{–}O_2)^s$, O_1 being the apical oxygen and O_2 the in-plane oxygen), tilt angle ($\varphi = (180\text{-}B\text{–}O_1\text{–}B)/2$), rotation angle $\omega = (180\text{-}B\text{–}O_2\text{–}B)/2$), and steric factor ($s = \overline{d(A-O)}/\sqrt{2}\overline{d(B-O)}$).

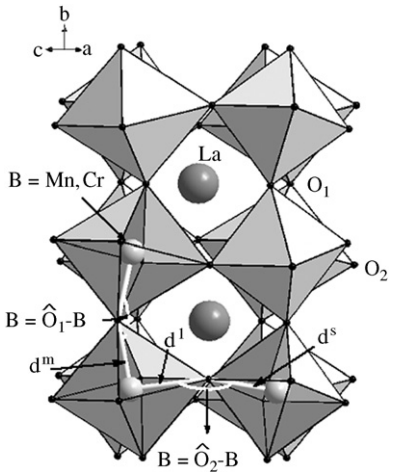

Fig. 3. Representation of the orthorhombic perovskite structure (S.G. *Pnma*). Following this picture is easy to recognize the parameters that characterized the structural distortions: tilt angle = $\varphi = (180\text{-}B\text{–}O_1\text{–}B)/2$; rotation angle = $\omega = (180\text{-}B\text{–}O_2\text{–}B)/2$; the three distances inside the octahedron: the long distance $d^l = d(B\text{–}O_2)^l$, the short one $d^s = d(B\text{–}O_2)^s$, and the medium distance $d^m = d(B\text{–}O_1)^m$.

Table 1 lists the cell parameters, the relationship between them (with the symmetry), and the cell volumes as a function of $3+\delta$. In Fig. 4, the evolution of cell parameters as a function of oxygen content ($3+\delta$) for $LaMn_{0.90}Cr_{0.10}O_{3+\delta}$ and $LaMn_{0.85}Cr_{0.15}O_{3+\delta}$ samples are compared. As it was observed for the former [22], a change in the relationships between cell parameters is also evidenced for the orthorhombic structure of $LaMn_{0.85}Cr_{0.15}O_{3+\delta}$ as a function of the oxygen content. For $0 \leqslant \delta < 0.05$, the O′ phase ($b/\sqrt{2} < c < a$) is found; for $0.05 \leqslant \delta \leqslant 0.06$, a becomes smaller than c (O″ phase: $b/\sqrt{2} < a < c$); for $0.06 < \delta < 0.09$, a is the smallest parameter giving rise to the O‴ phase ($a < b/\sqrt{2} < c$). For the highest values of oxygen content, the rhombohedral symmetry coexists with the orthorhombic one

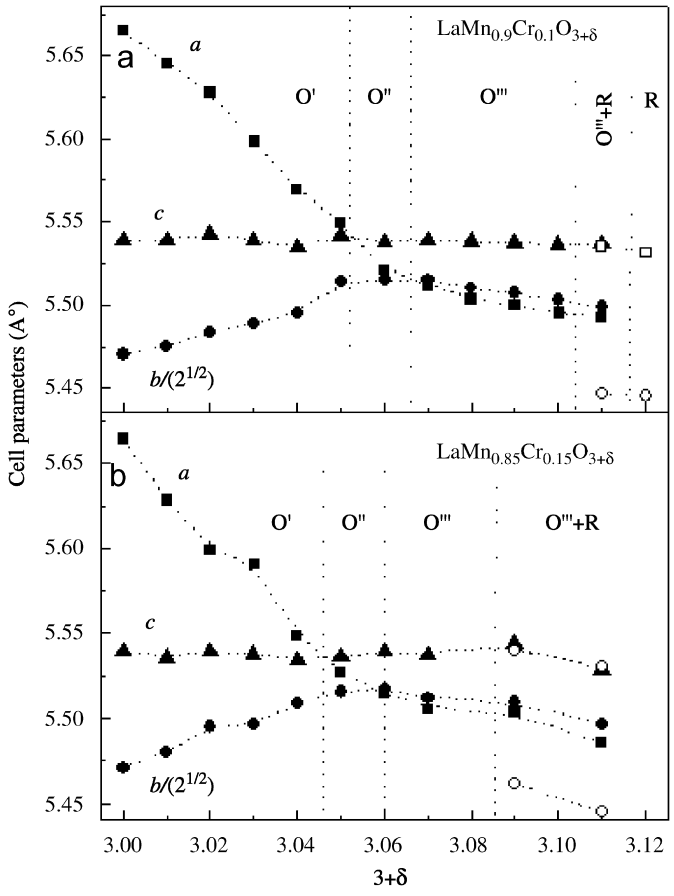

Fig. 4. Evolution of cell parameters for (a) $LaMn_{0.90}Cr_{0.10}O_{3+\delta}$ and (b) $LaMn_{0.85}Cr_{0.15}O_{3+\delta}$ compounds as a function of oxygen content (3+δ). The different orthorhombic regions and the biphasic field (orthorhombic and rhombohedral) are indicated showing the dependence with both, Cr and oxygen content.

forming a biphasic field. By comparison with the $LaMn_{0.90}Cr_{0.10}O_{3+\delta}$ compound, one observes that the phase boundaries O′|O″, O″|O‴ and O‴|(*R*+O‴) are shifted to lower δ values for the phase with 15% of Cr. Unlike $LaMnO_{3+\delta}$ and $LaMn_{0.90}Cr_{0.10}O_{3+\delta}$, purely rhombohedral symmetry was not obtained for $LaMn_{0.85}Cr_{0.15}O_{3+\delta}$ for any of the studied values of δ. It is expected that orthorhombic symmetry should be stabilized by the presence of the Cr^{3+} ions since $LaCrO_3$ has this symmetry at room temperature.

From Table 1, the decrease of the unit cell volume as the δ value increases is observed as a consequence of the decrease of the average ionic radius ($r^{4+}_{Mn} < r^{3+}_{Cr} < r^{3+}_{Mn}$ with $r^{4+}_{Mn} = 0.54$ Å, $r^{3+}_{Cr} = 0.615$ Å, and $r^{3+}_{Mn} = 0.65$ Å [28]).

In Table 2, the distances *B*–O, (d^m, d^l, and, d^s), the tilt (φ) and rotation (ω) angles are shown with their corresponding errors. Also, is included the steric factor (*s*) defined as $s = \overline{d(A-O)}/(\sqrt{2}\overline{d(B-O)})$ where $\overline{d(A-O)}$ and $\overline{d(B-O)}$ are the average *A* and *B* cation–anion distance, respectively. The main difference between the steric and the tolerance factor is that the former can be determined experimentally and for this reason it gives a more realistic evolution of the structural deformation with respect to the ideal perovskite.

The evolution of *B*–O distances for $LaMn_{0.85}Cr_{0.15}O_{3+\delta}$ and $LaMn_{0.9}Cr_{0.1}O_{3+\delta}$ is plotted in Fig. 5a. As expected, the structural distortion decreased with increasing the oxygen content. For $\delta \sim 0.05$, the cooperative JTD is lost (within the resolution of the XRD technique). Comparing with the sample with $x = 0.10$, there are no significant differences between the *B*–O distances. In addition, the octahedra become regular for a similar δ value. For the pure $LaMnO_{3+\delta}$ compound, the cooperative JTD is removed at $\delta \sim 0.06$, which is closed to the δ value for Cr-doped samples. The concentration of non-Jahn–Teller ions (in the *B* site) is 12%, 23%, and 27% for $x = 0$, 0.10, and 0.15 samples, respectively. It should be expected that as the concentration of non-Jahn–Teller increases, the suppression of the cooperative JTD as a function of oxygen content should occurs at lower values. However, our results suggest that the Jahn–Teller effect is not the only responsible of the octahedral distortion but the size of the Mn^{4+} also. As it is known, the stability of the perovskite structure is strongly dependent on the cation radius. For the *B*-site cation, the smallest radius accepted by this structure is 0.53 Å even when the tolerance factor is favorable [29]; this value is close to the Mn^{4+} radius. This could be the reason why structural distortions seem to be more sensitive to the Mn^{4+} concentration than the Cr^{3+} concentration.

In Fig. 5b, the changes in the tilt, φ, and rotation angle, ω, as a function of 3+δ are presented for both compositions. The evolution of these angles is related to changes in the magnetic properties. Both angles decrease as the oxygen content increases as a consequence of the gradual lost of the orthorhombic distortion. Comparing the φ evolution with that of the $LaMn_{0.90}Cr_{0.10}O_{3+\delta}$, clear differences are detected, in particular for low oxygen content. The difference between φ and ω is less in samples with $x = 0.15$ showing a more relaxed structure; also, the tilt angle decreases with the Cr content. Both results indicate the influence of the Cr concentration and thus it is expected that the magnetic behavior will differ from one compound to the other as the Cr concentration changes. As it will be shown, the FM interactions predominate over the AFM ones for $LaMn_{0.85}Cr_{0.15}O_{3+\delta}$ and this is evidenced by a smaller φ angle.

The obtained results for the evolution of both, the distances and the bond angles as a function of the Cr content, suggest that the presence of these ions mainly contribute to the tilt of the octahedra rather to its distortion, where the size of *B*-site ions plays also an important role.

3.3. Magnetotransport properties

The effect of variation of oxygen content on the magnetization (*M*) as a function of temperature (*T*), at $H = 0.01$ T, is shown in Fig. 6. This figure illustrates the complex nature of the $LaMn_{0.85}Cr_{0.15}O_{3+\delta}$ system. The stoichiometric sample shows a practically null M_{ZFC} revealing a frustrated system as a consequence of Cr inclusion on the *A*-type AFM structure. This frustration is, however, easily broken applying a small magnetic field as it is indicated by the fast growth of M_{FC}. As oxygen content is slightly increased, M_{ZFC} increases and displays a clear cusp of maximum magnetization at $3+\delta = 3.02$. The intensity of M_{ZFC} at low *T* for $3+\delta = 3.02$ is lower than that of $3+\delta = 3.01$ and constant, indicating spin freezing in the former sample $T < T_{cusp}$. This behavior would show that a glass phase is present together with substantial disorder, and is further supported by *M* vs. *H* curves plotted in Fig. 7 where the virgin curve remains outside the hysteresis loop. It has been reported that this kind of behavior is closely related to glass phases [30,31] and is an indicator of strong interactions inside the system which need to be overcome for the alignment of spins with *H*. Frustration and disorder are induced by the random distribution of Cr ions and, at the same time, interactions of different signs coexist. Ferromagnetism is induced inside the AFM matrix of the parent compound, $LaMnO_3$ by two mechanisms: the FM polarization of the Mn^{3+} nearest neighbors of Cr^{3+}, and the Mn^{3+}–O–Mn^{4+} DE interaction (which increases with oxygen content). So, the conditions giving rise to a glass

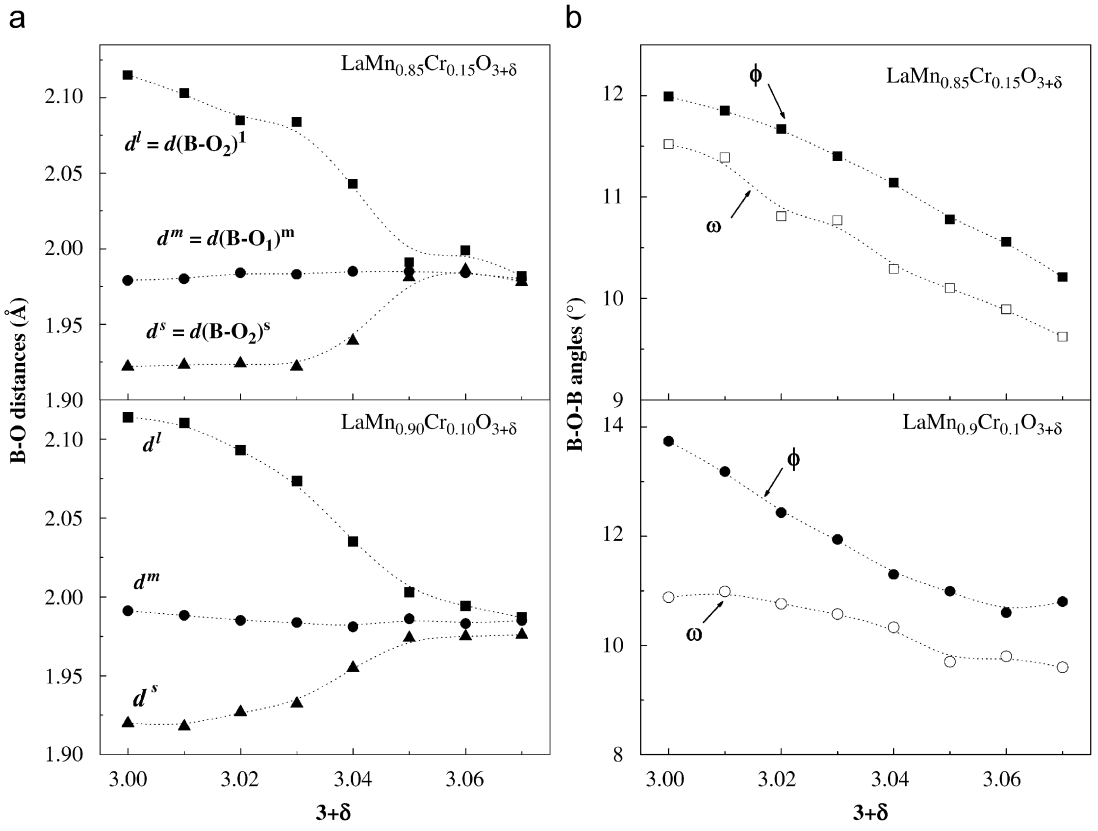

Fig. 5. Evolution of (a) *B*–O distances for the $LaMn_{0.90}Cr_{0.10}O_{3+\delta}$ and $LaMn_{0.85}Cr_{0.15}O_{3+\delta}$ compounds and (b) tilt (φ) and rotation (ω) angles for the same compositions, as a function of oxygen content.

phase are fulfilled. A close inspection of the hysteresis loops also reveals that, for the sample without Mn^{4+} ($\delta = 0$), the FM interaction is induced only by the presence of Cr^{3+}. This is pointed out through the fast magnetization and demagnetization of the system when the frustration is overcome. The shape of the loop does not correspond to a pure spin-glass phase, which could suggest the presence of more than one magnetic phase inside the sample.

As the oxygen content continues to increase, the FM interaction does as well, and for this reason the samples evolve to a ferromagnetic system for $\delta > 0.04$. *M* vs. *H* curves show that, for this range of oxygen content, the virgin curve loop remains inside the loop and the saturation occurs at lower field as δ increases.

The evolution of the magnetic transition temperature ($T_{N,C}$) and the magnetic moment (μ) as a function of the oxygen content ($3+\delta$) are shown in Fig. 8. The $T_{N,C}$ values were determined by differentiation of the magnetization curves showed in Fig. 6 and the μ values from the *M* vs. *H* curves at $T = 5$ K by extrapolation to $H = 0$. As it has been reported for the $LaMnO_{3+\delta}$ compounds [3], the critical temperature shows a minimum at $3+\delta$ values where the ferromagnetic phase dominates over the antiferromagnetic one. Above this oxygen content, the critical temperature increases with the δ value up to $\delta \sim 0.11$ where the AFM interaction Mn^{4+}–O–Mn^{4+} begins to play an important role. From Fig. 8, it is possible to see that the minimum disappears for the $LaMn_{0.85}Cr_{0.15}O_{3+\delta}$ samples suggesting the weakening of the long-range AFM phase over the FM one. By the comparison with the $LaMn_{0.90}Cr_{0.10}O_{3+\delta}$ system, one could suggest that the increase of the Cr content shows the FM character of the Mn^{3+}–O–Cr^{3+} interaction. At high oxygen content, there are no significant differences and both samples show similar saturated values for the critical temperatures without the maximum observed for the pure compound $LaMnO_{3+\delta}$. For both compositions, the maximum values of $T_{N,C}$ are reached at the less distorted structure (i.e. at the O‴ phase) where no clear differences inside the BO_6 octahedra are detected.

The evolution of the magnetic moment, μ, for $LaMn_{0.85}Cr_{0.15}O_{3+\delta}$ (Fig. 8b) presents an increase up to $\delta \sim 0.04$. At this value, the boundary between the O′ and O″ regions occurs. The same happens for the $LaMn_{0.90}Cr_{0.10}O_{3+\delta}$ samples with saturation at $\delta \sim 0.05$. For higher $3+\delta$ values and $x = 0.15$, μ also did not show significant changes. This behavior reflects the complex spin dynamic of this system where a mixture of different interactions are present ($Mn^{3+,4+}$–O–$Mn^{3+,4+}$, $Mn^{3+,4+}$–O–Cr^{3+}, Cr^{3+}–O–Cr^{3+}, Mn^{3+}–O–Mn^{4+}). Comparing the μ values, of $LaMn_{0.85}Cr_{0.15}O_{3+\delta}$ with those of $LaMn_{0.90}Cr_{0.10}O_{3+\delta}$, at $3+\delta > 3.04$, a clear decrease of the magnetic moment can be seen as a consequence of the increase in the Cr^{3+}–O–Mn^{4+} AFM interaction. If samples are prepared in this region ($3+\delta > 3.04$) without accurate control of the oxygen content or a similar concentration of Mn^{4+} is present as a consequence of an *A*-site doping, it would be possible to confuse the nature of the magnetic interactions. Thus, it could induce to associate that of Mn^{3+}–O–Cr^{3+} as AFM instead of FM because the presence of Mn^{4+}–O–Cr^{3+} AFM interaction. It should be noted that only 10% Mn^{4+} is necessary to observe this effect which is easily achieved with *A*-site doping.

In Fig. 9, the variation of the critical transition temperature $T_{N,C}$ as a function of the tilt angle, φ, is plotted for $3.00 \leqslant 3+\delta \leqslant 3.07$ (the region with only one symmetry present). $T_{N,C}$ varies significantly over a very short range, indicating the strong dependence of the magnetic interaction with structural distortions, in particular, with the tilt angle. Comparing this variation with that presented by $LaMn_{0.90}Cr_{0.10}O_{3+\delta}$ [22], it can be observed that the minimum around 12.5° is absent for $LaMn_{0.85}Cr_{0.15}O_{3+\delta}$. The tilt angles for $LaMn_{0.85}Cr_{0.15}O_{3+\delta}$ are lower than 12°. As was shown in Fig. 8, the $LaMn_{0.85}Cr_{0.15}O_{3+\delta}$ system does not present the typical minimum

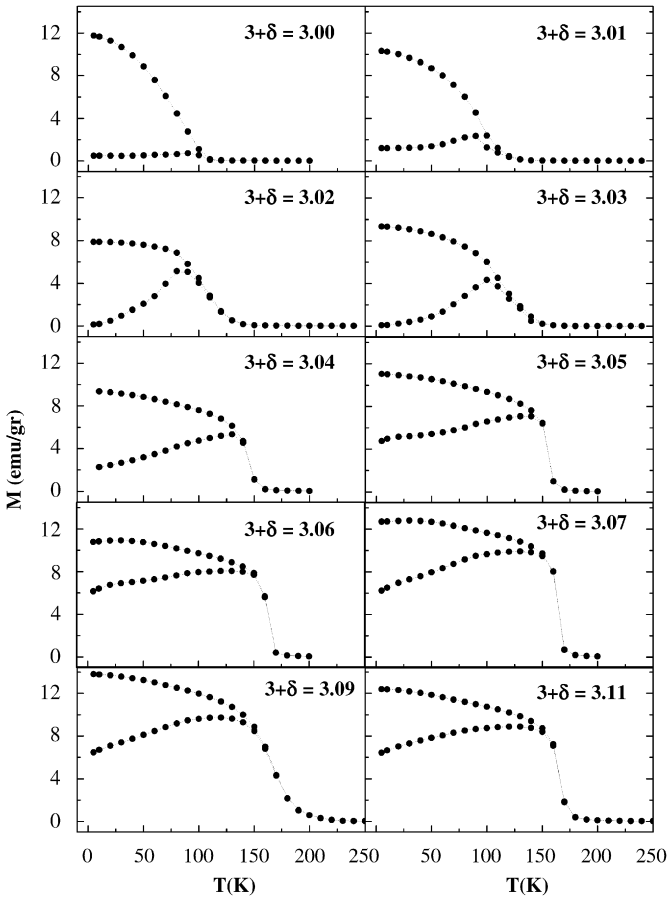

Fig. 6. M vs. T curves at $H = 0.01$ T for $LaMn_{0.85}Cr_{0.15}O_{3+\delta}$.

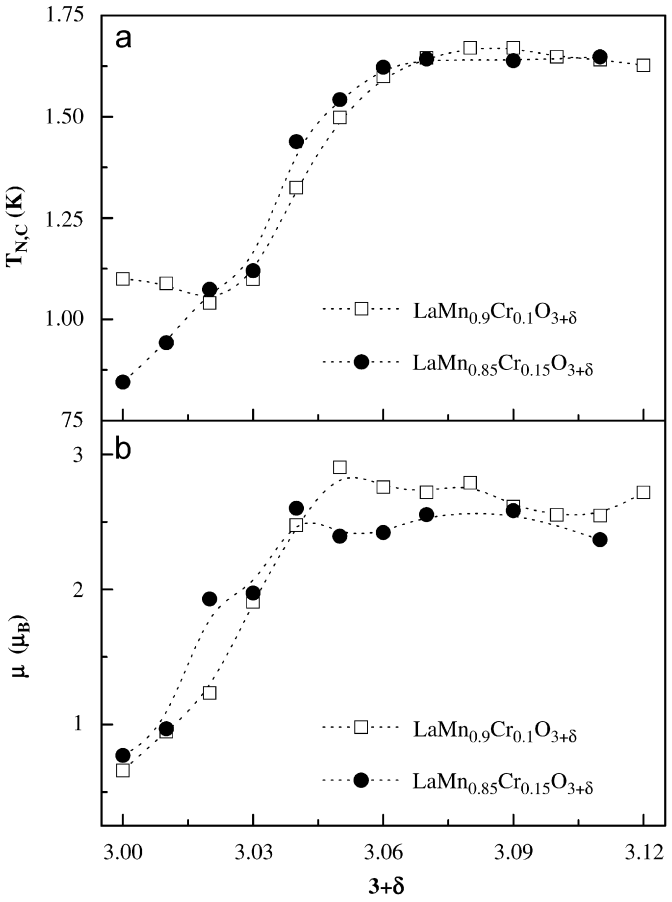

Fig. 8. Evolution of (a) critical temperature ($T_{N,C}$) and (b) magnetic moment (μ) (at $H = 5$ T and $T = 5$ K) vs. 3+δ for $LaMn_{0.85}Cr_{0.15}O_{3+\delta}$ and $LaMn_{0.90}Cr_{0.10}O_{3+\delta}$.

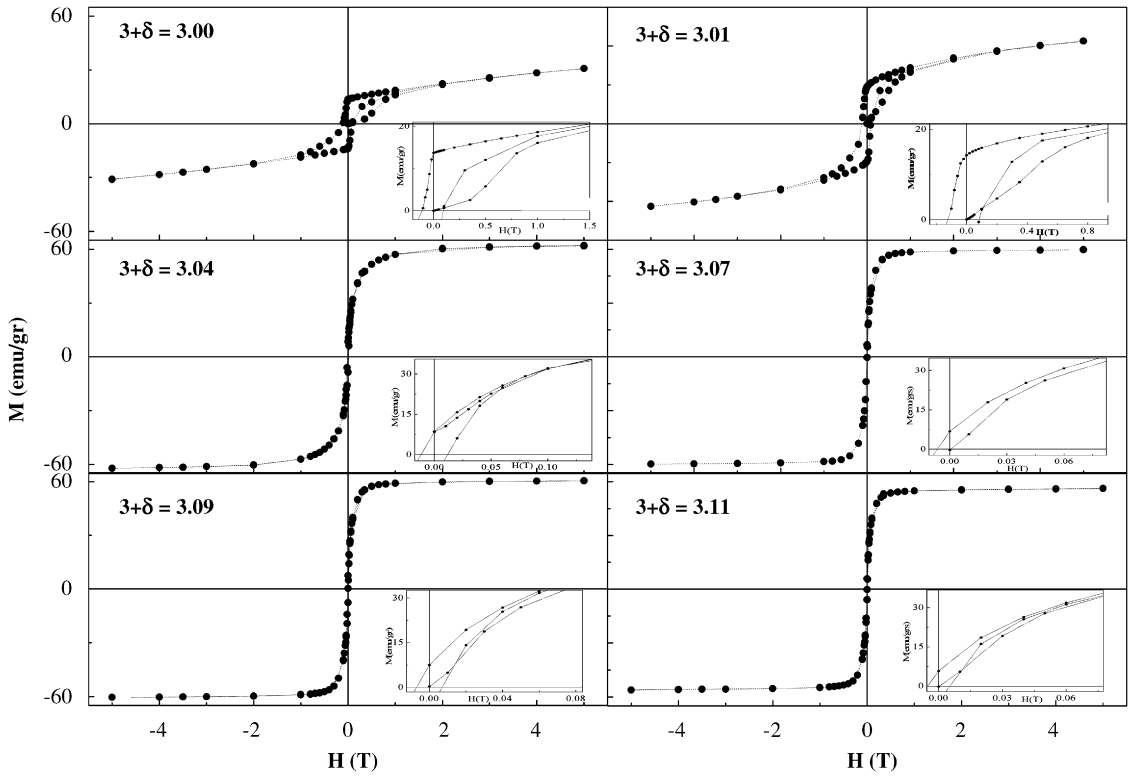

Fig. 7. M vs. H curves at $T = 5$ K for selected samples. In each inset, a detail of the coercitive field and the virgin curve is shown.

associated with the competition between AFM and FM interactions. Also, in Fig. 6, it is shown that for 3+δ~3.05 the FM character begins to be dominant in these samples. In earlier results, Huang et al. [32] reported for $LaMnO_{3+\delta}$ a FM phase for φ~9–10° and AFM one φ~12–13° which is in agreement with the results reported here. So, the magnetic behavior phase can be predicted by the variation of critical temperature with the tilt angle as follows: for $\varphi > 12°$ AFM is dominant, for $12° \leqslant \varphi \leqslant 11°$ the FM interaction begins to dominate over the AFM one and for lower φ values, the samples are majority FM. This result clearly demonstrates the close relationship between the structural distortion and the magnetic behavior especially that established between the tilt angle changes and the magnetic evolution.

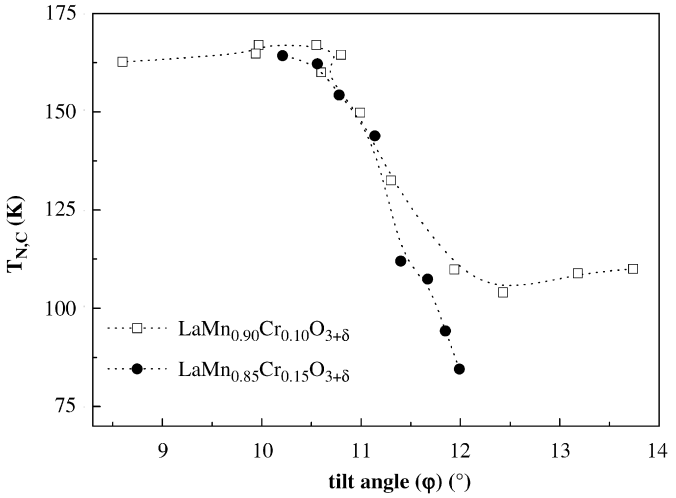

Fig. 9. Variation of the critical temperature ($T_{N,C}$) as a function of the tilt angle φ.

Curves of electrical resistance (R) with and without applied magnetic field as a function of T/T_C are shown in Fig. 10 for selected samples. Theses curves show the strong insulator character of these samples in all the studied range of oxygen content even when an external magnetic field is applied. This is in agreement with the results reported by Sun et al. [19] where they predict an insulator and semiconductor behavior in the ferromagnetic state for Cr-doped samples. As the 3+δ value increases, the resistance decreases as a consequence of the increase in the itinerant electron mobility along the paths established between Mn^{3+} and Mn^{4+} ions. As the oxygen content increases, the JTD and the splitting of the e_g levels decrease. One important effect in this kind of materials is the disorder induced by both, the structural random cation substitution and the high defect concentration introduced by the sample oxidation (cation vacancies). The presence of such defects generates localized states and changes the position of the mobility edge relative to the Fermi level. The insulator behavior exhibited by these samples suggests that the Fermi level is inside the region of localized states and therefore with an energy higher than that of the mobility edge. None of the

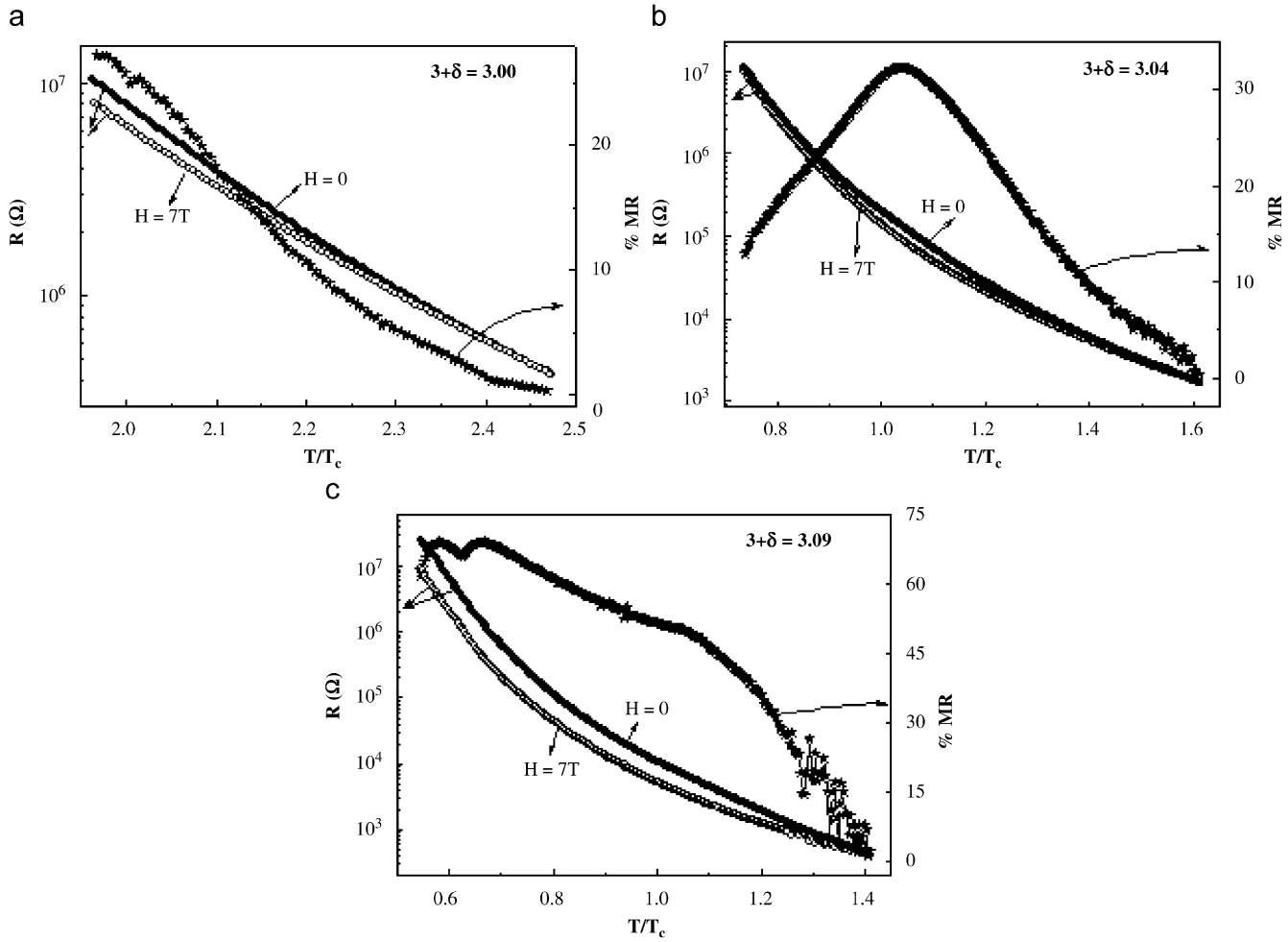

Fig. 10. Electrical resistance (R) vs. T curves for 3+δ = 3.00, 3.04, and 3.09 under $H = 0$ (close symbols) and 7 T (open symbols). The corresponding magnetoresistance MR curves are also plotted.

samples displayed the cross-over between the mobility edge and the Fermi level. This result demonstrates how an insulator material can exist even when the DE mechanism is present at least by the Mn^{3+}–O–Mn^{4+} interaction and the important role played by the disorder.

In all the samples, the effect of magnetoresistance is present even in the paramagnetic regime as is illustrated in (Fig. 10a) for the stoichiometric $LaMn_{0.85}Cr_{0.15}O_{3.00}$. By inspection of reported measurements in *A*-site-doped manganites, in general the MR effect is extended above the typical peak at $T \sim T_C$ [33,34]. For $3+\delta \leqslant 3.02$, the resistivity was higher than the range accepted by the experimental equipment making measurement possible only in the paramagnetic regime. High-temperature susceptibility of $LaMn_{0.85}Cr_{0.15}O_{3.00}$ showed a linear dependence with $1/T$ and the obtained effective magnetic moment was very close to the theoretical one [21]. This last result rules out the presence of clusters giving rise to the observed MR. In previously reported results on $LaMn_{1-x}B_xO_{3+\delta}$ (B = Zn, Li, Co, Ga, Sn), the absence of MR in the paramagnetic region [7–9] was found. Furthermore, in case of non-magnetic ions such as Ga and Sn (where magnetic interactions are clearly not established), MR effect was not found in the whole range of studied temperatures [7,9]. The parent stoichiometric compound $LaMnO_{3.00}$ does not present MR either in the whole range of temperatures [35] including the paramagnetic region. Because of all the above, in the Cr-doped samples it is necessary that the electron can jump from one ion to another (i.e. that an effective interaction has to be established between Mn^{3+} and Cr^{3+}). The super exchange interaction does not involve a real charge transfer, so the Mn^{3+}–O–Cr^{3+} interaction needs to be DE, which is in agreement with the model proposed by Morales et al. [21]. Similar behavior was found for the samples with $3+\delta = 3.01$, and 3.02. For $3.03 \leqslant 3+\delta < 3.09$ values, a peak close to T_C is found as happens for manganites in general (Fig. 10b). In this range, as δ increases, the maximum value of MR decreases but the peak broadens losing the character of peak for $3+\delta \geqslant 3.09$. For $3+\delta = 3.09$ (Fig. 10c) as the temperature decreases a change in the slope of the curves is found for $T/T_C \sim 1$. As the temperature continues decreasing, the MR increases. This effect shows that the MR is enhanced by increasing the Mn^{4+} concentration and, because the Cr^{3+} content is fixed, the absence of the peak close to T_C is also related to the increase of Mn^{4+}. This last effect could be a consequence of the increasing magnetic disorder induced by the competition of multiple interactions of different sign (which could give competition of phases), and also, for the structural disorder associated with cation vacancies. Even when the critical temperature and the magnetic moment are very similar in samples with $3+\delta \geqslant 3.05$, the electrical transport behavior, and more specifically the MR response, clearly indicates that the samples are different depending on the oxygen content.

4. Conclusions

In the present paper, a detailed magneto-structural study of the $LaMn_{0.85}Cr_{0.15}O_{3+\delta}$ system with $3.00 \leqslant 3+\delta \leqslant 3.11$ is reported as a continuation of the systematic studies on the $LaMn_{1-x}Cr_xO_{3+\delta}$ series. This study allowed the analysis of the effect of Cr^{3+} ions on the crystal structure and magnetic behavior of Cr-doped $LaMnO_3$ manganite changing, progressively both the Mn^{4+} and Cr^{3+} concentrations.

The substitution of Mn^{3+} by Cr^{3+} lowers the structural distortion as a consequence of the non-Jahn–Teller character of the Cr^{3+} ion and the difference in the ionic radii ($r^{3+}_{Mn} > r^{3+}_{Cr}$). By comparison with $LaMn_{0.90}Cr_{0.10}O_{3+\delta}$ it is possible to establish that, as the oxygen content varies, the effect of Cr^{3+} not only depends on the FM Cr^{3+}–O–Mn^{3+} interaction but also on the Cr^{3+}–O–Mn^{4+} one, and the Mn^{4+} ionic radius. On one hand, it is shown that for high oxygen content the effect of the Cr^{3+} concentration on the structural distortions seems to be disguised probably as a consequence of the small Mn^{4+} ionic radius. On the other hand, the magnetotransport properties change with Cr^{3+} content as a complex system due to the presence of multiple interactions ($Mn^{3+,4+}$–O–$Mn^{3+,4+}$, $Mn^{3+,4+}$–O–Cr^{3+}, Cr^{3+}–O–Cr^{3+}, Mn^{3+}–O–Mn^{4+}).

It has been proposed that the tilt angle, φ, could be used to predict the dominant magnetic phase in these kind of materials as it distinguishes between FM of AFM samples depending on its value. It has been clearly shown that the substitutions on the *B* site of the perovskite structure induce strong changes on the structural distortion but in the presence of large amounts of Mn^{4+} the effect of this ion dominates over the others. The evolution of structural properties as a function of oxygen content also reveals that magnetic properties are strongly dependent on small δ changes.

Once more, the importance of knowledge of the oxygen non-stoichiometry in order to analyze the magnetic behavior in a correct way has been shown. When both the oxygen content and the Cr^{3+} concentration increase, the AFM Cr^{3+}–O–Mn^{4+} and Cr^{3+}–O–Cr^{3+} interactions become relevant with a consequent decrease of the magnetization. These effects could be responsible for the misunderstanding on the role of Cr^{3+} in the magnetic interactions.

The existence of a DE interaction between Mn^{3+} and Cr^{3+} may explain the detection of MR in the sample free of Mn^{4+}, in the paramagnetic state. The same effect was observed for $LaMn_{0.90}Cr_{0.10}O_{3+\delta}$ system.

Acknowledgments

We thank Dr. Blas Alascio, Dr. Michael James, and Dr. L. Mogni for useful discussions and contributions to this manuscript. This work was supported by CNEA, CONICET, ANPCyT PICT 12-14493.

References

[1] J.B. Goodenough, Annu. Rev. Mater. Sci. 28 (1998) 1–27;
J.B. Goodenough, Magnetism and the Chemical Bond, Wiley, New York, 1963.
[2] A. Wold, R.J. Arnott, J. Phys. Chem. Solids 9 (1959) 176–180.
[3] F. Prado, R.D. Sánchez, A. Caneiro, M.T. Causa, M. Tovar, J. Solid State Chem. 146 (1999) 418–427.
[4] R. von Helmolt, J. Wecker, B. Holzapfel, L. Schultz, K. Samwer, Phys. Rev. Lett. 71 (1993) 2331–2333;
S. Jin, T.H. Tiefel, M. McCormack, R.A. Fastnacht, R. Ramesh, L.H. Chen, Science 264 (1994) 413–415;
J.M.D. Coey, M. Viret, S. von Molnár, Adv. Phys. 48 (1999) 167–294.
[5] C. Zener, Phys. Rev. 82 (1951) 403–405.
[6] B. Raveau, A. Maignan, R. Mahendiran, D. Khomskii, C. Martin, S. Hébert, M. Hervieu, R. Frésard, J. Phys. Chem. Solids 63 (6–8) (2002) 901–905.
[7] B. Vertruyen, D. Flahaut, S. Hébert, A. Maignan, C. Martin, M. Hervieu, B. Raveau, J. Magn. Magn. Mater. 280 (1) (2004) 75–83.
[8] S. Hébert, C. Martin, A. Maignan, R. Retoux, M. Hervieu, N. Nguyen, B. Raveau, Phys. Rev. B 65 (2002) 1044201–1044207.
[9] L. Morales, A. Caneiro, D. Vega, R. Zysler, H. Lanza, H.R. Mercader, J. Solid State Chem. 168 (2002) 100–109.
[10] U.H. Bents, Phys. Rev. 106 (1957) 225–230.
[11] R. Gundakaram, A. Arulraj, P.V. Vanitha, C.N.R. Rao, N. Gayathri, A.K. Raychaudhuri, A.K. Cheetham, J. Solid State Chem. 127 (1996) 354–358.
[12] A. Barnabé, A. Maignan, M. Hervieu, F. Damay, C. Martin, B. Raveau, Appl. Phys. Lett. 71 (1997) 3907–3909.
[13] C. Osthover, P. Grunberg, R. Arons, J. Magn. Magn. Mater. 181 (1998) 854–855.
[14] A. Maignan, C. Martin, F. Damay, M. Hervieu, B. Raveau, J. Magn. Magn. Mater. 188 (1998) 185–194.
[15] J. Dho, W.S. Kim, N.H. Hur, Phys. Rev. Lett. 89 (2002) 0272021–0272024.
[16] O. Cabezas, M. Long, C. Sevarac, M.A. Bari, C.M. Muirhead, M.G. Francesconi, C. Greaves, J. Phys.: Condens. Matter 11 (12) (1999) 2569–2578.
[17] F. Rivadulla, M.A. López-Quintela, L.E. Hueso, P. Sande, F. Rivas, R.D. Sánchez, Phys. Rev. B 62 (9) (2000) 5678–5684.

[18] N. Kallel, J. Dhahri, S. Zenni, E. Dhahri, M.U. Oumezzine, M. Ghedira, H. Vinvent, Phys. Stat. Sol. A 184 (2) (2001) 319–325.
[19] Y. Sun, W. Tong, X. Xu, Y. Zhang, Phys. Rev. B 63 (2001) 1744381–1744385.
[20] J. Deisenhofer, M. Paraskevopoulos, H.-A. Krug von Nidda, A. Loidl, Phys. Rev. B 66 (2002) 0544141–0544147.
[21] L. Morales, R. Allub, B. Alascio, A. Butera, A. Caneiro, Phys. Rev. B 72 (13) (2005) 1323131–1324134.
[22] L. Morales, A. Caneiro, J. Solid State Chem. 170 (2) (2003) 404–410.
[23] A. Serquis, F. Prado, A. Caneiro, Physica C 253 (1995) 339–350.
[24] Rodríguez Carvajal, Fullprof: Aprogram for Rietveld Refinement and Profile Matching Analysis of Complex Powder Diffraction Patterns, Laboratoire Léon Brillouin (CEA-CNRS).
[25] A. Caneiro, P. Bavdaz, J. Fouletier, J.P. Abriata, Rev. Sci. Instrum. 53 (1982) 1072–1076.
[26] A. Serquis, A. Caneiro, A. Basset, S. Short, J.P. Hodges, J. Jorgensen, Phys. Rev. B 63 (1) (2001) 145081–145089.
[27] C. Frontera, A. Caneiro, A.E. Carrillo, J. Oró-Solé, J.L. García-Muñoz, Chem. Mater. 17 (22) (2005) 5439–5445.
[28] R.D. Shannon, C.T. Prewitt, Acta Crystallogr. B 25 (1969) 925–946.
[29] C. Li, K.C.K. Soh, P. Wu, J. Alloys Compds. 372 (1–2) (2004) 40–48.
[30] G. Alejandro, D.G. Lamas, L.B. Steren, J.E. Gayone, G. Zampieri, A. Caneiro, M.T. Causa, M. Tovar, Phys. Rev. B 67 (6) (2003) 644241–644248.
[31] S. Senoussi, J. Phys. 45 (1984) 315–322.
[32] Q. Huang, A. Santoro, J.W. Lymm, R.W. Erwin, J.A. Bochers, J.L. Peng, R.L. Greene, Phys. Rev. B 55 (22) (1997) 14987–14999.
[33] M. García-Hernandez, A. de Andrés, J.L. Martínez, D. Sánchez Soria, L. Martín-Carrón, S. Taboada, J. Solid State Chem. 171 (1–2) (2003) 76–83.
[34] M.B. Salomon, M. Jaime, Rev. Mod. Phys. 73 (3) (2001) 583–629.
[35] R. Laiho, K.G. Lisunov, E. Lähderanta, V.S. Stamov, V.S. Zakhavlinskii, P.H. Colomban, P.A. Petrenko, Yu P. Stepanov, J. Phys.: Condens. Matter 17 (1) (2005) 105–118.